Krylov complexity for nonlocal spin chains

Aranya Bhattacharya,[1,*] Pingal Pratyush Nath,[2,†] and Himanshu Sahu[2,3,‡]

[1]*Institute of Physics, Jagiellonian University, Lojasiewicza 11, 30-348 Kraków, Poland*
[2]*Centre for High Energy Physics, Indian Institute of Science, C.V. Raman Avenue, Bangalore 560012, India*
[3]*Department of Instrumentation and Applied Physics, Indian Institute of Sciences, C.V. Raman Avenue, Bangalore 560012, Karnataka, India*

(Received 8 January 2024; accepted 18 February 2024; published 11 March 2024)

Building upon recent research in spin systems with nonlocal interactions, this study investigates operator growth using the Krylov complexity in different nonlocal versions of the Ising model. We find that the nonlocality results in a faster scrambling of the operator to all sites. While the saturation value of Krylov complexity of local integrable and local chaotic theories differ by a significant margin, this difference is much suppressed when nonlocal terms are introduced in both regimes. This results from the faster scrambling of information in the presence of nonlocality. In addition, we investigate the behavior of level statistics and spectral form factor as probes of quantum chaos to study the integrability breaking due to nonlocal interactions. Our numerics indicate that in the nonlocal case, late time saturation of Krylov complexity distinguishes between different underlying theories, while the early time complexity growth distinguishes different degrees of nonlocality.

DOI: 10.1103/PhysRevD.109.066010

I. INTRODUCTION

The study of operator growth using Krylov complexity (also referred to as "K-complexity") has emerged as a powerful framework for investigating the behavior of quantum systems and their underlying dynamics [1–3]. K-complexity is a measure of the delocalization of a local initial operator evolving under Heisenberg evolution with respect to the Hamiltonian [1–5]. It is conjectured to grow at most exponentially generically nonintegrable systems [1]. This exponential growth of K-complexity can be used to extract the Lyapunov exponent [1,2], establishing a connection with out-of-time-ordered-correlators (OTOC) [6,7]. Further studies have shown a relation between K-complexity and chaos in context of various models such as Ising models [8,9], Sachdev-Ye-Kitaev (SYK) models [5,10,11], quantum field theories [12–17], many-body localization system [18,19], and open quantum systems [20–24].

Among different systems, of particular interest are the so-called fast scramblers for which scrambling time is logarithmic in the number of degrees of freedom. The examples include black holes [6,25,26], conjectured to be the fastest scramblers in nature, SYK [27] and other related holographic models. The previous studies [28–31] suggest that local chaotic dynamics along with nonlocal interactions are sufficient to give rise to the phenomena termed as "fast scrambling." These developments have motivated the study of quantum information scrambling in nonlocal systems [32,33] as well as experimental proposal for probing fast scramblers with simpler models [30–32,34].

In this study, we characterize the growth of K-complexity in nonlocal systems. It has been established that K-complexity can distinguish between the integrable and chaotic regimes in local systems. To be precise, the complexity growth rate and saturation value are known to be significantly higher for chaotic systems as compared to the integrable ones [3,8,9]. Here, we ask the question of how these characteristics get modified once nonlocal interactions are turned on within these regimes. While chaotic systems with nonlocal interactions can exhibit fast scrambling properties, the nonlocal terms in the otherwise integrable cases are also expected to accelerate the operator growth and therefore begs some investigation as to whether the notions of local integrability and chaos remain distinguishable in the presence of nonlocality.

Apart from K-Complexity, we also study the two widely used measures to probe chaos: Level statistics (Appendix A 1) and spectral form factor (Appendix A 2). The symmetry-reduced level statistics is known to exhibit Poisson distribution for integrable regimes, while in chaotic regimes, it shows the Wigner-Dyson distribution [35–37]. On the other hand, the spectral form factor (SFF) is found to

*aranya.bhattacharya@uj.edu.pl
†pingalnath@iisc.ac.in
‡himanshusah1@iisc.ac.in

exhibit an explicit dip-ramp-plateau behavior for chaotic evolution in contrast to the integrable regime where higher amount of fluctuations wash out the dip-ramp-plateau behavior [38–40].[1] We study these quantities to compare their behavior in the presence of nonlocal terms in the Hamiltonian and analyse how the introduction of nonlocality changes their nature.

Our results indicate that with increasing degrees of nonlocality, the integrable evolution becomes similar to chaotic ones. We study the three diagnostics for characterizing chaos for various models which indicates that non locality apparently makes all regimes chaotic. However, a closer look at the plots reveals that nonlocal terms with local integrable operator evolution can still be distinguished from nonlocal terms with local chaotic operator evolution using K-complexity. Moreover, we also observe that the increase in nonlocality is captured by the initial growth rate of the K-complexity. To have a clearer understanding of how nonlocality changes behavior of Krylov complexity, we also study "mixed field" spin chains [33], where we vary the degree of nonlocality and study how it increases the slope of the Lanczos ascent.

The rest of the paper is structured as follows. In Sec. II, we briefly review the notion of K-complexity, and it's characteristics for local Hamiltonians, discussing both integrable and nonintegrable regimes. In Sec. III, we introduce several nonlocal models and discuss distinguished features present in the K-complexity profiles. Section III A consists of the numerical findings for nonlocality introduced to an otherwise local integrable and chaotic version of the transverse field Ising model. In Secs. III B and III C, we present the models and numerics when we deal with varying degrees of nonlocality by tuning a parameter in transverse field Ising model and XXZ spin chain respectively. Finally, we conclude in Sec. IV discussing the implications of our results. In the Appendix we study the remaining probes, namely the level statistics and the spectral form factor for both local and nonlocal models to be able to compare their behavior with Krylov complexity.

II. REVIEW FOR LOCAL HAMILTONIANS

In this section, we briefly review Krylov complexity and the features of operator growth for local Hamiltonians. As part of our exploration, we will focus on how this behaves within the context of the transverse-field Ising model, considering both integrable and nonintegrable scenarios. For our analysis, we will take the local Hamiltonian to be a one-dimensional transverse-field Ising model with open boundary conditions, which has the form,

$$H_{\mathrm{TFIM}} = -\sum_{j=1}^{N-1}\sigma_j^z\sigma_{j+1}^z - g\sum_{j=1}^{N}\sigma_j^x - h\sum_{j=1}^{N}\sigma_j^z, \qquad (1)$$

where g and h are the coupling parameters. When $h=0$, the Hamiltonian remains integrable for all values of g, as it can be mapped to the free-fermionic model [41]. However, when both g and h are nonzero, the system departs from integrability. To investigate the integrable regime, we set $g=1$ and $h=0$, while for the chaotic regime, we choose $g=-1.05$ and $h=0.5$ [42]. The model has a parity symmetry for all values of coupling parameters, and additional Z-reflection symmetry when $h=0$.

A. Operator dynamics in Krylov basis

We begin with a brief review of the operator dynamics in Krylov space [1–3]. Consider the evolution of an operator with seed $\mathcal{O}_0$ at $t=0$ under the time-independent Hamiltonian H. At any time t, the time-evolved operator $\mathcal{O}(t)$ under Heisenberg evolution can be written as

$$\mathcal{O}(t) = e^{iHt}\mathcal{O}_0 e^{-iHt} = e^{i\mathcal{L}t}\mathcal{O}_0 = \sum_{n=0}^{\infty}\frac{(it)^n}{n!}\mathcal{L}^n\mathcal{O}_0 \qquad (2)$$

where $\mathcal{L}$ is Liouvillian superoperator, which satisfies the relation $\mathcal{L}\mathcal{O} = [H,\mathcal{O}]$. This motivates the definition of Krylov space associated with the operator $\mathcal{O}$ as the minimal subspace of operator space that contains the time evolution of $\mathcal{O}$ at all times. Therefore, the Krylov space is obtained from repeated action of Liouvillian $\mathcal{L}^n\mathcal{O}$:

$$\begin{aligned}\mathcal{H}_{\mathcal{O}} &= \mathrm{span}\{\mathcal{L}^n\mathcal{O}\}_{n=0}^{\infty} \\ &= \mathrm{span}\{\mathcal{O},[H,\mathcal{O}],[H,[H,\mathcal{O}]],\ldots\}\end{aligned} \qquad (3)$$

Once the Krylov space is obtained, an orthonormal basis is then formed using a choice of inner product on the operator space. This is achieved using the Lanczos algorithm, an instance of the Gram-Schmidt process [1,43]. For our purpose, we will use the infinite-temperature inner product, also known as Frobenius inner product:

$$(\mathcal{A}|\mathcal{B}) = \frac{1}{D}\mathrm{Tr}[\mathcal{A}^\dagger\mathcal{B}], \qquad \|\mathcal{A}\| = \sqrt{(\mathcal{A}|\mathcal{A})}, \qquad (4)$$

where $D=\mathrm{Tr}[\mathbf{I}]$ is the trace of the identity matrix of appropriate dimension. In the orthonormal basis obtained from Lanczos iteration, the Liouvillian takes a tridiagonal form:

[1]This might vary from model to model. In some cases, an effective ramp appears, but it is not as evidently clear as it is for chaotic ones.

$$\mathcal{L} = \begin{pmatrix} 0 & b_1 & & & & 0 \\ b_1 & 0 & b_2 & & & \\ & b_2 & 0 & \ddots & & \\ & & \ddots & \ddots & b_{K-2} & \\ & & & b_{K-2} & 0 & b_{K-1} \\ 0 & & & & b_{K-1} & 0 \end{pmatrix} \tag{5}$$

where K is dimension of Krylov space, constrained to $1 \leq K \leq D^2 - D + 1$ [3]. Equation (5) can be recast into the following form,

$$\mathcal{L}|\mathcal{O}_n) = b_n|\mathcal{O}_{n-1}) + b_{n+1}|\mathcal{O}_{n+1}) \tag{6}$$

We can expand the time-evolving operator in the Krylov basis as:

$$|\mathcal{O}(t)) = \sum_{n=0}^{K-1} i^n \phi_n(t)|\mathcal{O}_n) \tag{7}$$

where $\phi_n(t)$ are time-dependent probability amplitudes associated with the Krylov chain. The wave functions satisfy the recursive differential equation, followed by the Heisenberg equation, which takes the form

$$\dot{\phi}_n(t) = b_n \phi_{n-1}(t) - b_{n+1}\phi_{n+1}(t) \tag{8}$$

where $\phi_{-1}(t) = 0$ and $\phi_n(0) = \delta_{n0}$. The unitarity of operator evolution implies a normalization condition on the probability amplitudes,

$$\sum_{n=0}^{K-1} |\phi_n(t)|^2 = 1 \tag{9}$$

In Eq. (8), we can think of the Lanczos coefficients b_n as the hopping amplitudes for the seed O_0 to traverse in the Krylov Space and ϕ_n as the probability amplitude associated with site n. The average position of the distribution on the Krylov chain is called K-complexity and is given by

$$C_K(t) = \sum_{n=0}^{K-1} n|\phi_n(t)|^2 \tag{10}$$

We can also define the complexity operator [44],

$$\mathcal{K} = \sum_{n=0}^{K-1} n|\mathcal{O}_n)(\mathcal{O}_n| \tag{11}$$

which plays the role of the position operator in the Krylov chain so that the Krylov complexity can be written as the expectation value of the complexity operator $\mathcal{K}$

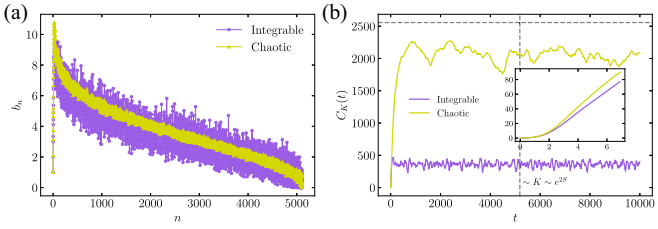

FIG. 1. (a) The Lanczos-sequence for the TFIM Hamiltonian in Eq. (1) computed for $L = 7$ spins with open boundary conditions for fixed parity $P = +1$ in integrable and chaotic limits. (b) Krylov complexity for TFIM Hamiltonian (1) computed for $L = 7$ spins with open boundary conditions for fixed parity $P = +1$ in Integrable and Chaotic limits. Outset: full-time range computed. Inset: zoom in at early times.

$$C_K(t) = (\mathcal{O}(t)|\mathcal{K}|\mathcal{O}(t)). \tag{12}$$

To study K-complexity we will use open boundary conditions and focus on a local operator $\mathcal{O}$ which respects the parity symmetry and keeps the computation within the chosen sector,

$$\mathcal{O} = S_i^z + S_{N-i+1}^z, \tag{13}$$

where i is chosen somewhere close to the center of the chain.[2] Figure 1 shows the Lanczos sequence b_n and K-complexity for TFIM Hamiltonian (1) computed for $L = 7$ for fixed parity $P = +1$ sector for the operator $\mathcal{O} = S_4^z$. The study of Lanczos sequence and Krylov complexity in integrable and chaotic limits have extensively been done in previous studies for different systems [8,46–48]. The Lanczos coefficient features sublinear growth in the integrable limit while linear growth in the chaotic limit, followed by saturation, and the descent, while K-complexity transitions from exponential growth at very early time to linear increase followed by saturation [3,8]. The saturation value of K-complexity is significantly large for local chaotic evolution as compared to the local integrable one. The suppressed complexity saturation of integrable cases results from higher fluctuations in Lanczos coefficients during the descent phase. This fluctuating descent period is dubbed as the Krylov localization.

[2]The operator is chosen so that it respects the parity symmetry (defined as in [45]) and keeps the computation within the chosen sector. The results deduced in this work remains unchanged even if i is varied in Eq. (13). However, as discussed in [8], the behavior of K-complexity is controlled by the statistics of the Hamiltonian spectrum and the structure of operator under consideration. For example, if the chosen operator has spread in all the sites from the beginning, the behavior of Krylov complexity might change as there is no scope for scrambling. Therefore, while the results can differ for an arbitrary seed operator, the conclusions remain invariant for any operator that respects the symmetries (parity here) of the Hamiltonian and has support in small number of sites to begin with so that it has enough scope to spread and scramble in the rest of the sites.

III. NONLOCAL MODELS AND NUMERICAL FINDINGS

In this section, we will study operator growth in nonlocal systems. We compare the results with the local counterpart to demonstrate the effect of nonlocality on these quantities. For these Hamiltonians, it is, in general, expected that due to nonlocal terms, the Liouvillian will also be nonlocal. Now, since the notion of integrability is believed to be closely related to locality [32,33], the evolution of the operator under the nonlocal Liouvillian is expected to show chaotic behavior even in the case when the local part of the Hamiltonian is integrable. Therefore it is expected that the nonlocal terms in the Hamiltonian will result in the loss of its integrability.

We study two types of nonlocal terms in this paper: (i) All-to-all couplings with the same interaction strength which we call the nonlocal transverse field Ising model, and (ii) All-to-all couplings with varying interaction strength, where the coupling between two sites decay as a power of the distance between the sites. We call this the transverse mixed field Ising model and by tuning the power, we vary the degree of nonlocality in this model.

A. Nonlocal transverse field Ising model

We consider the fast scrambling spin-1/2 Hamiltonian introduced in [31],

$$\mathcal{H} = \mathcal{H}_{\text{local}} - \frac{\gamma}{\sqrt{N}} \sum_{i<j} \sigma_i^z \sigma_j^z, \tag{14}$$

where σ_i^z is the Pauli z operator acting on site i and $\mathcal{H}_{\text{local}}$ is Hamiltonian with only local interactions. In our study, we will consider the local Hamiltonian as a one-dimensional transverse-field Ising model with open boundary conditions introduced in Sec. II. At this point, it is important to emphasize the terminology used throughout this literature. We will later observe from the results of operator growth as well as level-statistics and spectral form factor (discussed in the Appendixes A 1 and A 2), that nonlocality can break the integrability of the system. While referring to a system whose local part of the Hamiltonian in Eq. (14) is integrable, we will call it nonlocal integrable Hamiltonian even though nonlocality breaks integrability, and the model is no longer integrable.

We studied the nonlocal TFIM Hamiltonian with $L = 7$ sites and nonlocal parameter $\gamma = 0.5$. The numerical results for Lanczos-sequence and Krylov complexity are shown in Figs. 2 and 3. The global picture emerging from these results can be summarized in the following points:

(i) *Lanczos sequence.* The initial growth of Lanczos coefficients is faster for the nonlocal cases as compared to local cases (in both integrable and chaotic limits). While this accelerated growth is not prominently observable in smaller system sizes, it becomes distinctly apparent in larger system sizes as shown in Fig. 4. Note that the growth of the primary few Lanczos coefficients correspond to the pre-scrambling behavior. Hence a faster growth of primary Lanczos coefficients result in an higher exponent for the exponentially growing complexity before scrambling time. The peak value of the Lanczos sequence is more than that of the corresponding local case. The overall Lanczos profile for the nonlocal integrable case resembles the form of the local chaotic case. The fluctuations in the decaying part of the Lanczos sequence are also small for the nonlocal integrable case which results in a high saturation value of K-complexity.

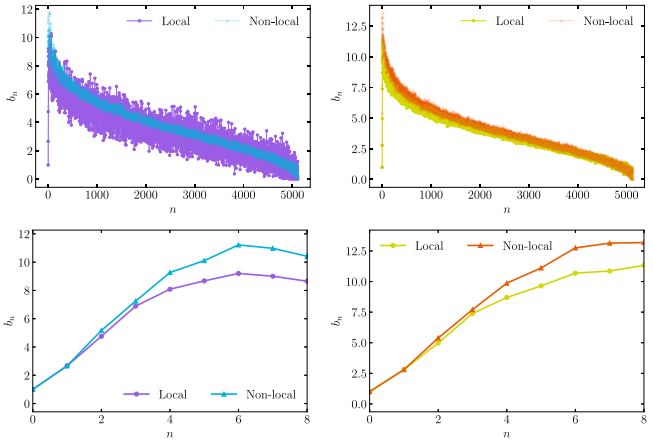

FIG. 2. Comparison between Lanczos-coefficients for local and nonlocal TFIM Hamiltonian with nonlocal parameter $\gamma = 0.5$, computed for $L = 7$ spins in the $P = +1$ sector for integrable and chaotic limits of local Hamiltonian. Top row: complete spectrum of Lanczos coefficients; Bottom row: initial Lanczos coefficients.

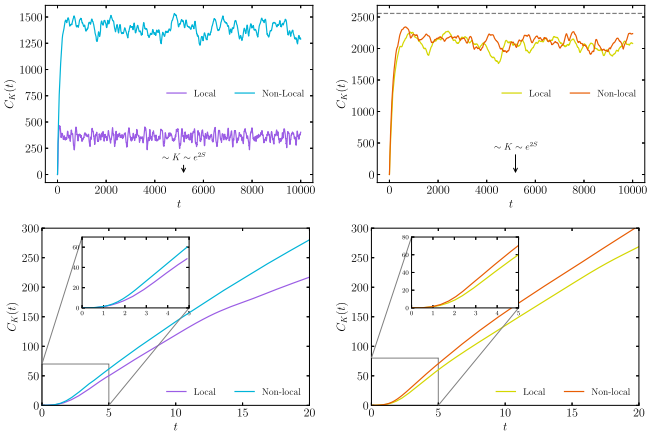

FIG. 3. Krylov complexity for TFIM Hamiltonian (1) computed for $L = 7$ spins with open boundary conditions for fixed parity $P = +1$, and nonlocality parameter $\gamma = 0.5$ in Left: integrable; Right: chaotic limits. Top: full-time range computed. Bottom: zoom in at early times.

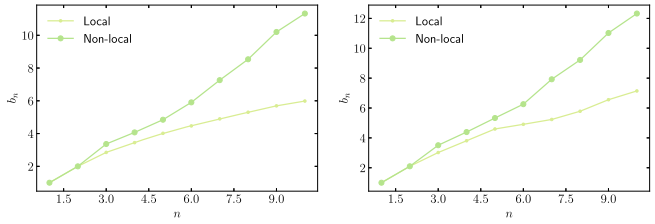

FIG. 4. Comparison between initial Lanczos-coefficients for local and nonlocal TFIM Hamiltonian with nonlocal parameter $\gamma = 0.5$, computed for $L = 12$ spins in the $P = +1$ sector for integrable and chaotic limits of local Hamiltonian. The Lanczos coefficients exhibit faster growth with nonlocal terms, especially evident in larger system sizes.

(ii) *K-complexity.* This shows a transition from exponential growth to linear increase starting from the scrambling time. This transition time is lower for nonlocal models in both integrable and chaotic regimes. Furthermore, the initial growth rate is also greater in nonlocal cases compared to their local counterparts. At exponentially late times the complexity saturates at half of the Krylov dimension for the chaotic cases local and nonlocal cases, since by then the operator is uniformly distributed over the Krylov basis. It is also worth noting that even after the introduction of nonlocal terms to the otherwise local integrable Hamiltonian, the complexity saturation value does not reach exactly the value of the local chaotic Hamiltonian. The saturation value for nonlocal terms + local integrable Hamiltonian is close to 1500 (much higher compared to local integrable which was 500) whereas the saturation value for nonlocal terms + local chaotic Hamiltonian is close to 2000 (almost similar to the local chaotic case). The late-time saturation value of the chaotic Hamiltonian is the same for both local and nonlocal cases, although the nonlocal chaotic Hamiltonian has a large initial growth compared to the local chaotic Hamiltonian.

B. Transverse mixed field Ising model

Consider the one-dimensional transverse mixed field Ising model of N spins with open boundary conditions

$$\mathcal{H}_\alpha = -\sum_{i<j} J_{ij}^{\alpha} \sigma_i^z \sigma_j^z - g\sum_i \sigma_j^x - h\sum_j \sigma_j^z \qquad (15)$$

where J_{ij}^{α} is interaction strength between spins at position i and j which assume to follow power law $1/\kappa \cdot J/|i-j|^{\alpha}$. Throughout our study, we take $J = 1$, and $\kappa = 1$. In previous studies [33], the information scrambling, using out-of-time-order correlators (OTOCs) as a probe, has been studied in such a model with a variation of nonlocal parameter α. It's shown that for $\alpha > 2$, the dynamics effectively resemble local dynamics, while for smaller exponents, the dynamics become nonlocal. Here, we will confine ourselves to studying the initial Lanczos sequence for the model with varying exponent α.

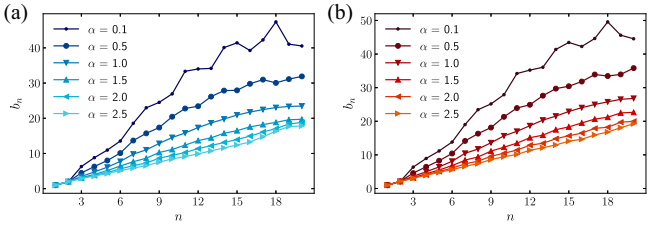

FIG. 5. The Lanczos-sequence for the transverse mixed field Ising model Hamiltonian in Eq. (15) computed for $L = 13$ spins with open boundary conditions for fixed parity $P = +1$ in (a) integrable and (b) chaotic limits with varying nonlocal exponent α values.

In Fig. 5, we showed the initial Lanczos coefficients b_n for $L = 13$ with varying exponent $\alpha \in \{0.1, 0.5, 1.0, 1.5, 2.0, 2.5\}$. The initial operator is chosen to be S_7^z. In both limits integrable and chaotic, we find the increasing slope and saturation value in initial growth with the decrease in exponent α and therefore increase in nonlocality. This ensures that the initial (prescrambling) growth rate of the Krylov complexity always increases in the presence of nonlocality (See Fig. 6). In Fig. 7, we showed the initial growth rate calculated using fit, $b_n = \delta \frac{n}{ln[n]} + c$ (for 1D systems, as conjectured in [1]) in initial Lanczos coefficients.

The saturation value of the late-time Krylov complexity is controlled by the amount of fluctuations in the Lanczos coefficients as reported in [9,22]. Fluctuations are more for

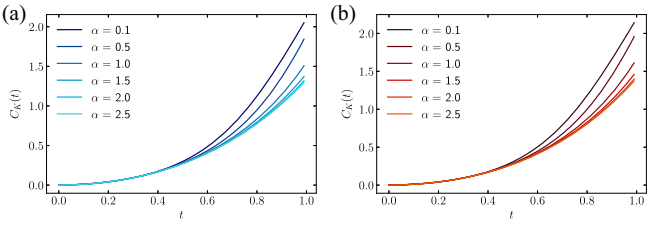

FIG. 6. Krylov complexity for the transverse mixed field Ising model Hamiltonian in Eq. (15) computed for $L = 13$ spins with open boundary conditions for fixed parity $P = +1$ in (a) integrable and (b) chaotic limits with varying nonlocal exponent α values.

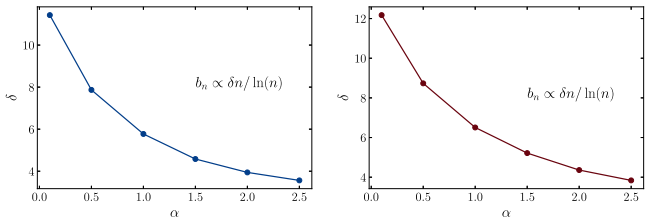

FIG. 7. The growth rate δ plotted for different nonlocal exponent α values for Lanczos coefficients in Fig. 5.

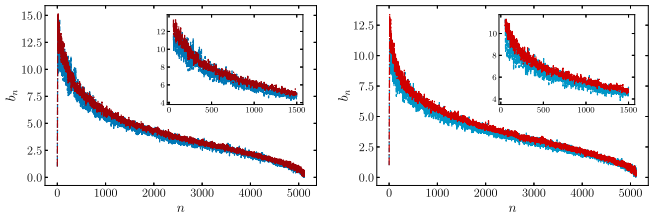

FIG. 8. The complete Lanczos-sequence is calculated for mixed-field TFIM for $L = 7$ spins in the $P = +1$ sector. The comparison between the coefficients is shown for integrable and chaotic values with Left: $\alpha = 0.5$; Right: $\alpha = 1$. The inset shows that the fluctuations for integrable parameter value (blue) are larger compared to chaotic parameter value (red). These larger fluctuation in large b_n leads to suppression of K-complexity for integrable parameter values even for nonlocal model.

integrable parameter values and this phenomenon is dubbed as the Krylov localization. We notice that although nonlocal terms in the Hamiltonian increase the initial growth in Lanczos coefficients for both integrable and chaotic parameter values, the fluctuations in later Lanczos coefficients is still comparatively more for the integrable parameter values. This is shown in Fig. 8 for two choices of the nonlocal exponent α of the mixed TFIM model. As a result, the late time saturation value of Krylov complexity in Fig. 9 distinctly differentiates the nature of the underlying integrable and chaotic theories even in the nonlocal models. In Fig. 9, the left figure shows the complexity saturation for various nonlocal + integrable cases while the same is shown for nonlocal + chaotic cases for various α. While the late-time saturation value indeed distinguishes whether the underlying theory is integrable or chaotic, it remains insensitive to the magnitude of the nonlocal exponent α. Nevertheless, as we noted earlier, the pre-scrambling growth of both Lanczos coefficients as well as the Krylov complexity serves as a clear indicator distinguishing between the nonlocal behaviors associated with different values of the exponent (Fig. 5).

C. Mixed field XXZ Hamiltonian

In this section, we will introduce mixed-field XXZ Hamiltonian analogous to mixed-field TFIM. The XXZ Hamiltonian contains nearest-neighbor interaction terms which are used to describe the behavior of a system of interacting spin-1/2 particles in a magnetic field and the Hamiltonian can be written as,

$$H_{\mathrm{XXZ}} = \frac{1}{4}\sum_{i=1}^{N-1} J(\sigma_i^x\sigma_{i+1}^x + \sigma_i^y\sigma_{i+1}^y) + \frac{J_{zz}}{4}\sigma_i^z\sigma_{i+1}^z. \quad (16)$$

The XXZ Hamiltonian commutes with total spin operator M in the z-direction and is also invariant under reflection with respect to the edge of the chain, i.e., under parity operator P. In previous studies [8,49–55], it was shown that the integrability can be broken by addition local term

$$H_d = S_j^z. \quad (17)$$

The mixed field XXZ is an extension of the XXZ Hamiltonian where we add varying nonlocal strength analogous to the case of mixed field TFIM.

$$\mathcal{H}_{XXZ}^{(\alpha)} = \frac{1}{4}\sum_{i=1}^{N-1} J_{ij}^{\alpha}(\sigma_i^x\sigma_{i+1}^x + \sigma_i^y\sigma_{i+1}^y) + \frac{\tilde{J}_{ij}^{\alpha}}{4}\sigma_i^z\sigma_{i+1}^z \quad (18)$$

where J_{ij}^{α} and $\tilde{J}_{ij}^{\alpha}$ are interaction strength between spins at position i and j. These follow power law behavior, $1/\kappa \cdot J/|i-j|^{\alpha}$, and $1/\kappa \cdot J_{zz}/|i-j|^{\alpha}$ respectively. Note that this model reduces to local XXZ model in the limit $\alpha \to \infty$. We consider the following nonlocal interpolating Hamiltonian:

$$\mathcal{H}_{\mathrm{nonlocal}} = \mathcal{H}_{XXZ}^{(\alpha)} + \epsilon_d H_d. \quad (19)$$

In our study, we will consider $H_d = S_{(N+1)/2}^z$, and therefore, both the symmetry-breaking terms keep the symmetries intact. In further calculations, we fix $J = 1$, and $J_{zz} = 1.1$ for all cases.

We study the initial Lanczos sequence and K-complexity for $L = 12$ with varying exponent α for zero and nonzero value of ϵ_d (See Figs. 10 and 11). The initial operator $\mathcal{O}$ is

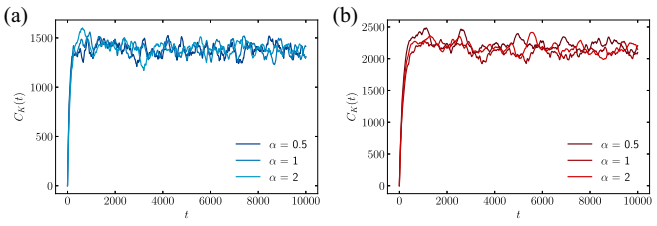

FIG. 9. Late time Krylov complexity for the transverse mixed field Ising model Hamiltonian computed for $L = 7$ spins with open boundary conditions for fixed parity $P = +1$ in (a) integrable and (b) chaotic limits with varying nonlocal exponent α values.

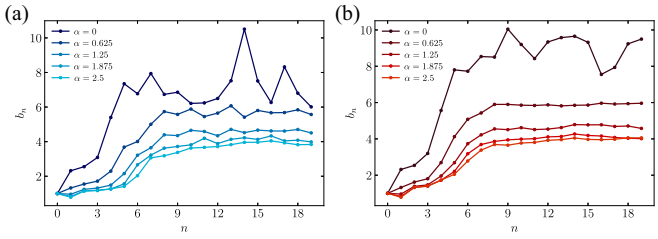

FIG. 10. The Lanczos-sequence for the transverse mixed field XXZ model Hamiltonian in Eq. (15) computed for $L = 12$ spins with open boundary conditions for fixed parity $P = +1$ and $M = 5$ in (a) $\epsilon_d = 0$ and (b) $\epsilon_d = 0.5$ limits with varying nonlocal exponent α values. The initial operator is chosen to be $S_6^z + S_7^z$.

chosen such that it respects the two symmetries of the model, i.e., parity and total spin in z-direction

$$\mathcal{O} = S_i^z + S_{N-i+1}^z \tag{20}$$

where i is chosen to be near the center of the chain. We find the increasing slope and saturation value in initial growth with the decrease in exponent α and, therefore increase in nonlocality. These results are in agreement with the results presented in the main text for the mixed-field TFIM model and, therefore, reflect the universality of the result. We assert that the initial (prescrambling) growth rate of the Krylov complexity is always increased in the presence of nonlocality.

IV. CONCLUSIONS

To conclude, we have explored the behavior of K-complexity in nonlocal spin chains. The purpose of this study is to delineate what kind of novel features this quantity can capture in the presence of nonlocal couplings. Over the course of this work, the K-complexity has emerged as a quantity of prime importance as it shows signs of nonlocality in the system. Let us recount the major findings in the following.

A. Discussion of results

Lanczos sequence. The saturation and initial growth of Lanczos coefficients is greater in nonlocal TFIM Hamiltonian relative to the local case, which reflects the faster information scrambling in nonlocal systems. The local chaotic dynamics, along with long-range nonlocal interactions, are sufficient to give rise to fast scrambling. This is because the Lanczos sequence for chaotic Hamiltonian with local interactions saturates at a comparatively smaller value than its nonlocal chaotic counterpart. The large saturation value of Lanczos coefficients are the result of nonlocal interactions in the system, but they can equivalently be said to be the result of fast scrambling as well. The fluctuation in the nonlocal cases is also suppressed, which is a result of integrability breaking due to nonlocal interaction. This results in a higher saturation value of Krylov complexity.

Krylov complexity. Apart from common features of Krylov complexity, such as the transition from exponential growth to linear and the late time saturation, we find that the initial time growth rate is greater in nonlocal cases, indicating the onset of fast scrambling in the system. The higher growth rate in Krylov complexity for the nonlocal cases is a result of the initial faster growth of Lanczos coefficients in nonlocal cases due to the nonlocal interaction. Furthermore, since nonlocality results in integrability breaking, we also find a large saturation value in Krylov complexity satisfying the bound in terms of the Krylov dimension. It is important to note that although the nonlocal interactions with the integrable local part of Hamiltonian show level statistics that of a chaotic model, it does not attain K-complexity saturation value similar to that of a chaotic case. In terms of associated Lanczos coefficients, the nonlocal integrable case has larger fluctuations as compared to the local chaotic case. It is noteworthy that even the introduction of the nonlocality does not make the integrable model fully chaotic. On the other hand, when similar nonlocal terms are introduced in the otherwise local chaotic model, the late-time saturation value does not change much compared to the local chaotic model. However, the initial growth of complexity is faster in this case also. We reach similar conclusions through our study in the mixed field Ising and XXZ models. While the initial complexity growth acts as a probe of the degree of nonlocality (different α), the late-time saturation value only probes whether the underlying local theory ($\alpha > 2$) is integrable or not.

In summary, our findings provide compelling evidence that operator growth, as characterized by K-complexity, exhibits a significantly greater magnitude in nonlocal systems when compared to their local counterparts. An increase in the nonlocality parameter leads to a heightened scrambling rate in the system, as evident from both the Lanczos spectrum and the K-complexity profile. Furthermore, our observations indicate that the escalation of the nonlocality parameter results in the breakdown of integrability and a transition toward chaotic behavior in the system. The integrability breaking due to nonlocal interaction is also evident from our study level statistics as well as spectral form factor (see Appendixes A 1 and A 2).

B. Outlook

In future work, we would like to understand the relation between nonlocality and fast scrambling better. This requires a careful investigation of scrambling time which is logarithmic in system size for fast scramblers, therefore requires investigation on system with large sizes.[3] It would be interesting find the degree of nonlocality require for fast scramblers by studying model with power-law decaying interactions. In Ref. [56], the authors shown that the fast scrambling is prohibited in models with a generic all-to-all term with prefactor $\sim 1/N^\gamma$ if $\gamma > 1/2$. It would be interesting if this bound can be verified from operator growth using K-complexity.

Although all-to-all interactions are thought to be essential for fast scrambling [31], certain systems demonstrate fast scrambling even in the absence of such interactions [57]. These models consider spin chains with next-to-nearest neighbor interactions in a specified combination of some sectors. The spread of quantum information in similar models with mild nonlocality are studied in literature [58]. These study show that although nonlocality increases the

[3]We leave this for future study due to the lack of resources to perform computation for higher dimensions.

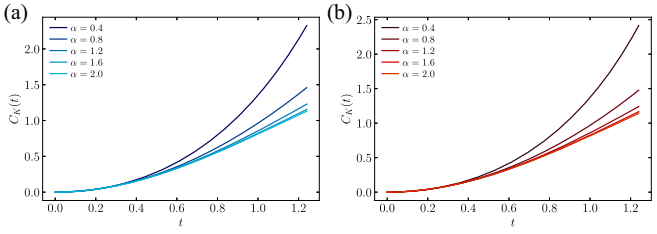

FIG. 11. Krylov complexity for the transverse mixed field XXZ model Hamiltonian in Eq. (15) computed for $L = 12$ spins with open boundary conditions for fixed parity $P = +1$ and $M = 5$ in (a) $\epsilon_d = 0$ and (b) $\epsilon_d = 0.5$ limits with varying nonlocal exponent α values.

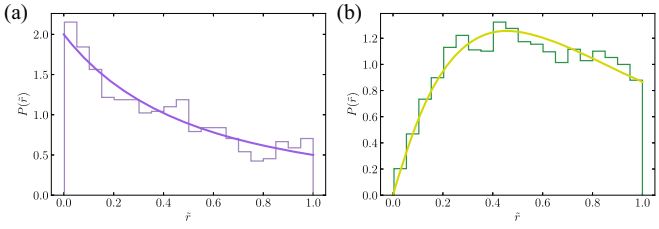

FIG. 12. Probability distribution functions of the $\tilde{r}$ statistics for fixed Z-reflection symmetry blocks and parity block of the Hamiltonian (1), computed for $L = 13$ spins in the $P = +1$, and $z = +1$ sector in (a) integrable and (b) chaotic limits. The results are obtained from averaging over 100 ensembles with ϵ drawn from normal distribution with mean 0 and deviation 10^{-4}. The mean level spacing ratio obtained for the integrable and chaotic limits are 0.38733 and 0.53433 respectively.

rate of information spreading, but in lattice models these rates are suppressed. An extension of this work may consider K-complexity in such mild nonlocal models.

ACKNOWLEDGMENTS

We wish to thank Sumilan Banerjee, Rathindra Nath Das, Bidyut Dey, Johanna Erdmenger, Mario Flory, Aaron Friedman, Michal Heller, Chethan Krishnan, Manas Kulkarni, Subroto Mukherjee, Pratik Nandy, and Aninda Sinha for various useful discussions and comments about this and related works. The work of A. B. is supported by the Polish National Science Centre (NCN) Grant No. 2021/42/E/ST2/00234.

All authors contributed equally to this work. The authors of this paper were ordered alphabetically.

APPENDIX: OTHER PROBES OF CHAOS: LEVEL STATISTICS AND SPECTRAL FORM FACTOR

1. Level statistics

In quantum chaos, random matrix theory (RMT) is a powerful tool that accurately describes the spectral statistics of quantum systems whose classical counterparts exhibit chaotic behavior. For quantum Hamiltonians associated with integrable classical systems, the Berry-Tabor conjecture suggests that their level statistics follow a Poisson distribution [35].

However, for quantum Hamiltonians whose classical counterparts are chaotic, the Bohigas-Giannoni-Schmit conjecture proposes that their level statistics should fall into one of the three classical ensembles of RMT [36]. These ensembles correspond to Hermitian random matrices with independently distributed entries as follows:

(i) Gaussian orthogonal ensemble (GOE): Corresponding to systems with real random variables as matrix entries.
(ii) Gaussian unitary ensemble (GUE): Corresponding to systems with complex random variables as matrix entries.
(iii) Gaussian symplectic ensemble (GSE): Corresponding to systems with quaternionic random variables as matrix entries.

These ensembles provide a robust framework for understanding the statistical behavior of quantum systems with chaotic classical dynamics. Consider e_n be an ordered set of energy levels and the nearest-neighbor spacing, $s_n = e_{n+1} - e_n$. Now, define the ratios $\tilde{r}_n$ as

$$\tilde{r}_n = \frac{\min(s_n, s_{n-1})}{\max(s_n, s_{n-1})} = \min\left(r_n, \frac{1}{r_n}\right) \tag{A1}$$

where

$$r_n = \frac{s_n}{s_{n-1}}. \tag{A2}$$

The distribution $P(r)$ for random matrix ensembles Wigner ensembles (GOE, GUE, and GSE) is shown to [37]

$$P(r) = \frac{1}{Z_\beta} \frac{(r + r^2)^\beta}{(1 + r + r^2)^{1+(3/2)\beta}} \tag{A3}$$

with Z_β the normalization constant. The Wigner ensembles are distinguished by their Dyson index ($\beta = 1$, 2 and 4 respectively) in distribution Eq. (A3). For a Poissonian distribution of level-spacings, the distribution of r is given by

$$P(r) = \frac{1}{(1 + r)^2} \tag{A4}$$

The distribution $P(r)$ and $P(\tilde{r})$ are related to one another by $P(\tilde{r}) = 2P(r)\Theta(1 - r)$. The mean value $\langle\tilde{r}\rangle$ associated with different distribution (listed in below table) can be used to distinguish between integrable and chaotic systems.

Ensembles	Poisson	GOE	GUE	GSE
$\langle\tilde{r}\rangle$	$2\ln 2 - 1$	$4 - 2\sqrt{3}$	$2\frac{\sqrt{3}}{\pi} - \frac{1}{2}$	$\frac{32}{15}\frac{\sqrt{3}}{\pi} - \frac{1}{2}$
	≈ 0.38629	≈ 0.53590	≈ 0.60266	≈ 0.67617

Results. In Fig. 12, we showed the probability distribution functions of the $\tilde{r}$ statistics of the local TFIM

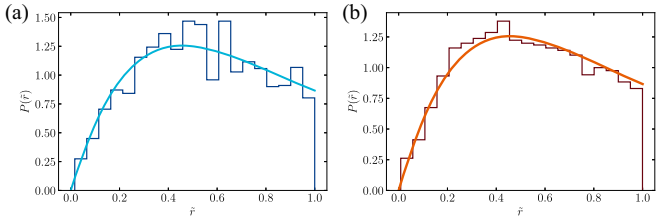

FIG. 13. Probability distribution functions of the $\tilde{r}$ statistics for fixed Z-reflection symmetry blocks and Parity block of the nonlocal Hamiltonian (1), computed for $L = 13$ spins in the $P = +1$, and $z = +1$ sector and nonlocality parameter $\gamma = 0.5$ in (a) integrable and (b) chaotic limits of local Hamiltonian. The results are obtained from averaging over 100 ensembles with ϵ drawn from a normal distribution with mean 0 and deviation 10^{-4}. The mean level spacing ratio obtained for integrable and chaotic limits are 0.53784 and 0.52738 respectively.

Hamiltonian (1) in integrable and chaotic regimes. We compare the results for both $P(\tilde{r})$ and $\langle\tilde{r}\rangle$ with the analytical results for Poisson and GOE symmetry class. The numerical result are in good agreement with those of analytical.

In Fig. 13, we showed the probability distribution function of the $\tilde{r}$ statistics for nonlocal TFIM Hamiltonian (see Sec. III A) computed for $L = 13$ spins. As reported in [31], we find that nonlocality term changes the integrable model to chaotic for $|\gamma| \gtrsim 0.25$.

In Fig. 14, we shown level statistics distribution for transverse mixed field Ising model discussed in Sec. III B for varying nonlocal exponent α. It is clear from here that it is hard to distinguish these different degrees of nonlocality from the level statistics, while the initial growth rate of K-complexity can quite clearly distinguish them. The reason is that in K-complexity, we can distinguish between different degrees of nonlocality during the prescrambling regime. At the same time, the level statistics can capture only the details about the nature of the spectrum, and there is no way to make such a timewise distinction.

2. Spectral form factor

To compute the spectral form factor, we use the analytically continued partition function

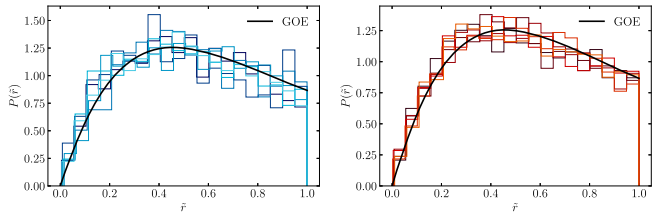

FIG. 14. Probability distribution functions of the $\tilde{r}$ statistics for Transverse mixed field Ising model for varying exponent α. Refer Sec. III B for parameter values.

$$Z(\beta, t) \equiv \mathrm{Tr}(e^{-\beta H - iHt}) \tag{A5}$$

of the usual partition function $Z(\beta) = \mathrm{Tr}(e^{-\beta H})$. The function $Z(\beta, t)$ is an erratic function of time and, therefore oscillates largely at late times. The fluctuations are studied by considering the normalized squared quantity, the so-called spectral form factor (SFF) [38–40].

$$\begin{aligned} g(\beta, t) &= \left|\frac{Z(\beta, t)}{Z(\beta)}\right|^2 \\ &= \frac{1}{Z(\beta)^2}\sum_{m,n} e^{-\beta(E_m+E_n)} e^{i(E_m-E_n)t} \end{aligned} \tag{A6}$$

where E_n is eigenvalue of energy eigenstate $|n\rangle$. The long-time average can be written as

$$\lim_{T\to\infty}\frac{1}{T}dt\left|\frac{Z(\beta, t)}{Z(\beta)}\right|^2 = \frac{Z(2\beta)}{Z(\beta)^2} \tag{A7}$$

where we assumed the system Hamiltonian H to be nondegenerate. Due to the erratic nature of $Z(\beta, t)$, usually the ensemble average over large Hamiltonians is considered. We define disorder-averaged analogs of SFF in Eq. (A6) as

$$g_{\mathrm{ann}}(\beta, t) = \frac{\mathbb{E}[|Z(\beta, t)|^2]}{\mathbb{E}[|Z(\beta, 0)|^2]} \tag{A8}$$

$$g_{\mathrm{que}}(\beta, t) = \mathbb{E}\left[\left|\frac{Z(\beta, t)}{Z(\beta, 0)}\right|^2\right] \tag{A9}$$

which are called annealed SFF and quenched SFF, respectively. Throughout this paper, we use the notatin $\mathbb{E}[.]$ to denote the ensemble average. In this work, we will be working with annealed SFF along with $\beta = 0$, meaning that we are taking the disorder average separately in the numerator and denominator. We will further call $g_{\mathrm{ann}}(\beta, 0) = g(t)$, sometime this itself is referred to as the spectral form factor, which has information about the correlations of eigenvalues at different energy separations. To understand the time profile of SFF, we split the $|\mathbb{E}[|Z(\beta, t)|^2]$ into two parts as

$$\begin{aligned} &|\mathbb{E}\mathrm{Tr}(e^{-iH(\beta+it)})|^2 \\ &\quad + (\mathbb{E}[|\mathrm{Tr}(e^{-iH(\beta+it)})|^2] - |\mathbb{E}\mathrm{Tr}(e^{-iH(\beta+it)})|^2) \end{aligned} \tag{A10}$$

The first term is a disconnected part of the SFF, which comes solely from the average density of states. The second part is a connected part which contains the information on the correlation between energy levels. According to random matrix universality, an ensemble of quantum chaotic Hamilontians will generically have the same *connected* SFF as the canonical Gaussian ensembles

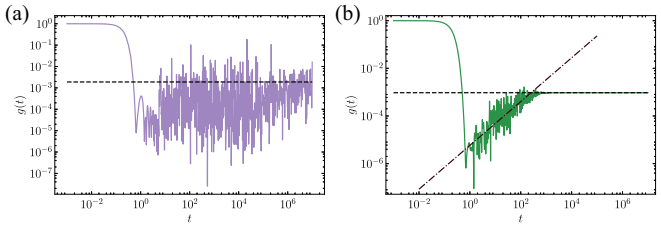

FIG. 15. A log-log plot of TFIM Hamiltonian SFF $g(t;\beta=0)$, plotted against time for $L=11$ in (a) integrable and (b) chaotic limits. The value at late times, which is equal to plateau height g_p, matches with $Z(2\beta)/Z(\beta)^2$ (shown in black dashed line). The average is taken over 50,000 samples drawn from the random value of ϵ taken from a normal distribution with mean $\mu=0$ and standard deviation $\sigma=0.01$ in case of chaotic limit. The dash-dot line shows the linear fit in the ramp region, showing the linear increase.

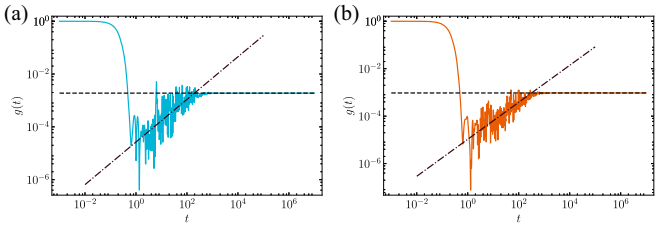

FIG. 16. A log-log plot of nonlocal TFIM Hamiltonian SFF $g(t;\beta=0)$, plotted against time for $L=11$, and $\gamma=0.5$ in (a) integrable and (b) chaotic limits of local TFIM Hamiltonian. The value at late times, which is equal to plateau height g_p, matches with $Z(2\beta)/Z(\beta)^2$ (shown in black dashed line). The average is taken over 50,000 samples drawn from the random value of ϵ taken from normal distribution with mean $\mu=0$ and standard deviation $\sigma=0.01$. The dash-dot line shows the linear fit in the ramp region, showing the linear increase.

of RMT. The conjectured universal profile of the SFF of the GUE contains three distinct regimes [40,59,60]:

(i) Initially the value drops quickly, through a region we call the *slope*, to a minimum, which is called the *dip*. The early time dip in profile comes from the disconnected part of the SFF therefore, its precise shape is nonuniversal. It is the result of loss of constructive interference in different terms of $\mathrm{Tr}e^{-iH(\beta+it)}$ which acquire different phase factors as t increases.

(ii) After a dip, the values increase roughly linearly which is what we call the *ramp*. The ramp is due to the repulsion between eigenvalues that are far apart in the spectrum, which is also well known in quantum chaotic systems. Therefore a linear ramp is often taken as a defining signature of quantum chaos.

(iii) The *plateau*, which occurs at late times, results from the discreteness of the spectrum.

The overall profile for GOE and GSE symmetry class also follows a slope-dip-ramp-plateau pattern apart from a few details, such as the shape of the ramp and the plateau. For example, the SFF of the GUE symmetry class has a sharp kink, while in the GOE symmetry class, the kink is smoothed [59].

Results. In Fig. 15, we showed the behavior of SFF of the TFIM Hamiltonian (1), where an average is taken for the chaotic case. In the calculation of SFF for integrable cases, we did not consider the disorder average since the model is no longer integrable with the addition of disorder. It is still a "free-fermion model" in the sense that it is bilinear in fermion operators. But it is not integrable anymore. While there are still an extensive number of conserved quantities, they are no longer quasilocal, so we expect to see chaotic behavior. In our calculation, we do find that the addition of disorder in integrable cases gives rise to a ramp in the SFF profile. In previous studies [61], it is shown that integrable systems such as rectangular billiards, SYK_2 model, and square-mod systems don't show ramps in their SFF profile. However, the emergence of a ramp-like feature has been demonstrated after averaging over the ensemble in the SYK_2 model. In Appendix A 1, we see that the model follows the statistics of the GOE symmetry class in the chaotic limit; therefore, we would expect such a profile to be the same as that of GOE symmetry class. In other words, in chaotic limit, we find slope-dip-ramp-plateau profile as evident from the figure.

In Fig. 16, we show the SFF of nonlocal TFIM Hamiltonian for $L=11$, and $\gamma=0.5$ in the integrable and chaotic limits. We took the disordered average over 50,000 samples drawn from the random value of ϵ. We find slope-dip-ramp-plateau patterns in both limits, integrable and chaotic, indicating that the non local interaction makes the Hamiltonian chaotic even when its local counterpart is in the integrable regime. It is also worth noting that there is no clear way to distinguish between the two nonlocal plots here. On the other hand, as described in the main text, by looking at the saturation values of the nonlocal K-complexity plots, we can still distinguish between which was integrable and which was not in the local version.

[1] D. E. Parker, X. Cao, A. Avdoshkin, T. Scaffidi, and E. Altman, Phys. Rev. X **9**, 041017 (2019).
[2] J. L. F. Barbón, E. Rabinovici, R. Shir, and R. Sinha, J. High Energy Phys. 10 (2019) 264.
[3] E. Rabinovici, A. Sánchez-Garrido, R. Shir, and J. Sonner, J. High Energy Phys. 06 (2021) 062.
[4] A. Dymarsky and A. Gorsky, Phys. Rev. B **102**, 085137 (2020).
[5] S.-K. Jian, B. Swingle, and Z.-Y. Xian, J. High Energy Phys. 03 (2021) 014.
[6] J. Maldacena, S. H. Shenker, and D. Stanford, J. High Energy Phys. 08 (2016) 106.
[7] A. Avdoshkin and A. Dymarsky, Phys. Rev. Res. **2**, 043234 (2020).
[8] E. Rabinovici, A. Sánchez-Garrido, R. Shir, and J. Sonner, J. High Energy Phys. 07 (2022) 151.
[9] E. Rabinovici, A. Sánchez-Garrido, R. Shir, and J. Sonner, J. High Energy Phys. 03 (2022) 211.
[10] B. Bhattacharjee, P. Nandy, and T. Pathak, J. High Energy Phys. 08 (2023) 099.
[11] S. He, P. H. C. Lau, Z.-Y. Xian, and L. Zhao, J. High Energy Phys. 12 (2022) 070.
[12] P. Caputa and S. Datta, J. High Energy Phys. 12 (2021) 188; 09 (2022) 113(E).
[13] S. Khetrapal, J. High Energy Phys. 03 (2023) 176.
[14] A. Kundu, V. Malvimat, and R. Sinha, J. High Energy Phys. 09 (2023) 011.
[15] H. A. Camargo, V. Jahnke, K.-Y. Kim, and M. Nishida, J. High Energy Phys. 05 (2023) 226.
[16] A. Avdoshkin, A. Dymarsky, and M. Smolkin, arXiv: 2212.14429.
[17] J. Erdmenger, S.-K. Jian, and Z.-Y. Xian, J. High Energy Phys. 08 (2023) 176.
[18] F. B. Trigueros and C.-J. Lin, SciPost Phys. **13**, 037 (2022).
[19] P. H. S. Bento, A. del Campo, and L. C. Céleri, arXiv:2312 .05321.
[20] A. Bhattacharya, P. Nandy, P. P. Nath, and H. Sahu, J. High Energy Phys. 12 (2022) 081.
[21] B. Bhattacharjee, X. Cao, P. Nandy, and T. Pathak, J. High Energy Phys. 03 (2023) 054.
[22] A. Bhattacharya, P. Nandy, P. P. Nath, and H. Sahu, J. High Energy Phys. 12 (2023) 066.
[23] C. Liu, H. Tang, and H. Zhai, Phys. Rev. Res. **5**, 033085 (2023).
[24] B. Bhattacharjee, P. Nandy, and T. Pathak, J. High Energy Phys. 01 (2024) 094.
[25] Y. Sekino and L. Susskind, J. High Energy Phys. 10 (2008) 065.
[26] N. Lashkari, D. Stanford, M. Hastings, T. Osborne, and P. Hayden, J. High Energy Phys. 04 (2013) 022.
[27] S. Sachdev and J. Ye, Phys. Rev. Lett. **70**, 3339 (1993).
[28] B. Swingle, G. Bentsen, M. Schleier-Smith, and P. Hayden, Phys. Rev. A **94**, 040302 (2016).
[29] J. Marino and A. M. Rey, Phys. Rev. A **99**, 051803 (2019).
[30] G. Bentsen, T. Hashizume, A. S. Buyskikh, E. J. Davis, A. J. Daley, S. S. Gubser, and M. Schleier-Smith, Phys. Rev. Lett. **123**, 130601 (2019).
[31] R. Belyansky, P. Bienias, Y. A. Kharkov, A. V. Gorshkov, and B. Swingle, Phys. Rev. Lett. **125**, 130601 (2020).
[32] Z. Li, S. Choudhury, and W. V. Liu, Phys. Rev. Res. **2**, 043399 (2020).
[33] D. Wanisch, J. D. A. Espinoza, and S. Fritzsche, Phys. Rev. B **107**, 205127 (2023).
[34] M. Tezuka, O. Oktay, E. Rinaldi, M. Hanada, and F. Nori, Phys. Rev. B **107**, L081103 (2023).
[35] J. Marklof, in *European Congress of Mathematics*, edited by C. Casacuberta, R. M. Miró-Roig, J. Verdera, and S. Xambó-Descamps (Birkhäuser Basel, Basel, 2021), pp. 421–427, https://link.springer.com/chapter/10.1007/978-3-0348-8266-8_36.
[36] O. Bohigas, M. J. Giannoni, and C. Schmit, Phys. Rev. Lett. **52**, 1 (1984).
[37] Y. Y. Atas, E. Bogomolny, O. Giraud, and G. Roux, Phys. Rev. Lett. **110**, 084101 (2013).
[38] J. S. Cotler, G. Gur-Ari, M. Hanada, J. Polchinski, P. Saad, S. H. Shenker, D. Stanford, A. Streicher, and M. Tezuka, J. High Energy Phys. 05 (2017) 118; 09 (2018) 2(E).
[39] A. del Campo, J. Molina-Vilaplana, and J. Sonner, Phys. Rev. D **95**, 126008 (2017).
[40] M. Winer, R. Barney, C. L. Baldwin, V. Galitski, and B. Swingle, J. High Energy Phys. 09 (2022) 032.
[41] S. Sachdev, *Quantum Phase Transitions*, 2nd ed. (Cambridge University Press, Cambridge, England, 2011).
[42] M. C. Bañuls, J. I. Cirac, and M. B. Hastings, Phys. Rev. Lett. **106**, 050405 (2011).
[43] Z. Bai, J. Demmel, J. Dongarra, A. Ruhe, and v. d. H. Vorst, *Templates for the Solution of Algebraic Eigenvalue Problems: A Practical Guide*, 1st ed. (Society for Industrial and Applied Mathematics, 2000), https://epubs.siam.org/doi/abs/10.1137/1.9780898719581.
[44] N. Hörnedal, N. Carabba, A. S. Matsoukas-Roubeas, and A. del Campo, Commun. Phys. **5**, 207 (2022).
[45] K. Joel, D. Kollmar, and L. F. Santos, Am. J. Phys. **81**, 450 (2013).
[46] N. Iizuka and M. Nishida, J. High Energy Phys. 11 (2023) 065.
[47] A. Bhattacharyya, D. Ghosh, and P. Nandi, J. High Energy Phys. 12 (2023) 112.
[48] H. A. Camargo, V. Jahnke, H.-S. Jeong, K.-Y. Kim, and M. Nishida, arXiv:2306.11632.
[49] L. F. Santos, J. Phys. A **37**, 4723 (2004).
[50] L. F. Santos and A. Mitra, Phys. Rev. E **84**, 016206 (2011).
[51] O. S. Barišić, P. Prelovšek, A. Metavitsiadis, and X. Zotos, Phys. Rev. B **80**, 125118 (2009).
[52] M. Brenes, E. Mascarenhas, M. Rigol, and J. Goold, Phys. Rev. B **98**, 235128 (2018).
[53] M. Brenes, J. Goold, and M. Rigol, Phys. Rev. B **102**, 075127 (2020).
[54] M. Pandey, P. W. Claeys, D. K. Campbell, A. Polkovnikov, and D. Sels, Phys. Rev. X **10**, 041017 (2020).
[55] A. Gubin and L. F. Santos, Am. J. Phys. **80**, 246 (2012).
[56] C. Yin and A. Lucas, Phys. Rev. A **102**, 022402 (2020).
[57] K. Ikeda, arXiv:2105.13589.
[58] S. Eccles, W. Fischler, T. Guglielmo, J. F. Pedraza, and S. Racz, J. High Energy Phys. 12 (2021) 019.
[59] G. Cipolloni, L. Erdős, and D. Schröder, Commun. Math. Phys. **401**, 1665 (2023).
[60] E. Brézin and S. Hikami, Phys. Rev. E **55**, 4067 (1997).
[61] S. Das, C. Krishnan, A. P. Kumar, and A. Kundu, J. High Energy Phys. 01 (2023) 153.